IET Microwaves, Antennas & propagation

Special issue Call for Papers

Be Seen. Be Cited. Submit your work to a new IET special issue

"Green antenna technologies enabling sustainable RFID and IoT systems"

Guest Editors: Riccardo Colella, Almudena Rivadeneyra, Massimo Merenda and Antonio Alex-Amor

Read more

The Institution of Engineering and Technology

Received: 3 March 2022 | Revised: 18 October 2022 | Accepted: 19 October 2022

IET Microwaves, Antennas & Propagation

DOI: 10.1049/mia2.12316

ORIGINAL RESEARCH

Design of a Low temperature cofired ceramic wideband WideScan antenna array for millimetre-wave applications

Fuguo Zhu[1,2] | **Yuefei Wang**[2] | **Jinping Zhang**[1,2] | **Lei Sun**[1,2] | **Zhipeng Zhou**[1,2] | **Steven Gao**[3]

[1]Science and Technology on Antenna and Microwave Laboratory, Nanjing, China

[2]The 14th Research Institute, CETC, Nanjing, China

[3]School of Engineering and Digital Arts, University of Kent, Canterbury, UK

Correspondence

Fuguo Zhu, Science and Technology on Antenna and Microwave Laboratory, Nanjing, 210039, China.
Email: zhu.fuguo@hotmail.com

Abstract

The design, fabrication, and measurement of a 7 × 7 mm-wave array antenna have been presented for 5G communications. The substrate integrated waveguide (SIW)-fed antenna element is formed of four parts: a rectangular radiating patch, a coupling slot cut onto the broadwall of the SIW, a transition layer, and a feeding layer at the bottom. The bandwidth and radiation efficiency has been improved by embedding an air cavity below the radiating patch, as the effective dielectric constant of the substrate is reduced. Moreover, a prototype has been fabricated and measured to verify the design principles. The finite array operating over 23–28 GHz has achieved active voltage standing wave ratios of less than 2 and 2.5 in the E- and H-planes while scanning up to 45° respectively. Compared with the theoretical ideal gain, the average gain drop of the measured embedded element gain is 0.73dB.

KEYWORDS

millimetre-wave antenna array, wideband widescan array

1 | INTRODUCTION

The research on millimetre-wave antennas has attracted increasing attention in recent years due to the development of 5G communication. As the interests in 5G millimetre-wave antennas have been increasing in industries and academia, the 26 and 28-GHz bands are two candidates for 5G communications [1]. Therefore, wideband millimetre-wave antenna arrays covering these frequency bands are preferred as they are suitable for various communication applications. In addition, the choice of the substrate for designing millimetre-wave antennas needs to be taken into consideration. Low temperature cofired ceramic (LTCC) technology is an excellent candidate for designing millimetre-wave antennas due to its merits of multilayer configuration, flexible metallisation, and low fabrication tolerance. Moreover, compared with conventional multilayer print circuit board (PCB) technology, the LTCC technology is easier in the realisation of blind vias and across-layer connection by vias [2]. In the literature, the LTCC technology has been widely utilised for designing millimetre-wave antenna and arrays [3–5]. A fin-shaped heatsink antenna array operating at 60 GHz has been fabricated by 3-D printing and LTCC technologies [3]. A 3-D printed fin-shaped heatsink structure is soldered on a LTCC substrate with a chip mounted on the bottom. The LTCC technology has also been utilised to design a 60 GHz dual-polarized high-gain antenna array [4]. The high gain has been achieved by expanding to a two-dimensional array form while the two independent polarisations are realised by using orthogonal coupling slots excited by substrate integrated waveguide (SIW) power dividers. An integration of S/Ka/D-band antennas in a LTCC package has been proposed in ref. [5]. Three types of antennas, including microstrip patch, grid array, and step-profiled horn operating at different frequencies are compactly assembled in the same substrate.

However, the high permittivity and Q-factor of the LTCC substrate at millimetre-wave frequency leads to significant losses and narrow bandwidth. Several methods have been proposed to increase the bandwidth and reduce the losses of LTCC-based antenna [6–8]. The uni-planar electromagnetic band-gap has been placed around radiating patches to suppress the mutual coupling between antennas and overcome the problem of surface wave [6]. An increase of up to 4.5 and

2.3dB has been achieved in the gain for a single element and for a 16-element array, respectively, while the electromagnetic band gap structure has occupied a large area. In ref. [7], open air cavities between radiating patches have been employed to reduce the losses by surface waves. The gain of the array has been enhanced by 1–2dB while the discontinuous of the structure may disrupt the current distributions. Furthermore, an ideal method is to embed an air cavity in LTCC to lower the effective dielectric constant, which leads to an increased bandwidth and gain enhancement [8]. In addition, the impedance bandwidth and maximum gain of a 60-GHz patch array on LTCC have been improved significantly by embedding a large cavity underneath the radiating patches [9]. The drawback of this method is the high risk of deformation.

The enhancement of the impedance and gain of the LTCC millimetre-wave array has been further investigated in this paper. By embedding a cavity under each radiating patch of an array, the effective dielectric constant is reduced, indicating anf increased bandwidth and a lower loss. To ensure the reliability, small holes have been drilled in the top layer of LTCC substrate to avoid any deformation of the cavity due to the pressure difference. A prototype of a 7 × 7 LTCC millimetre-wave array has been designed, fabricated and measured to validate the design principles.

2 | ANTENNA ELEMENT DESIGN

The structure and geometry of the proposed wideband antenna element are shown in Figure 1. The utilised substrate is LTCC Ferro A6-M with $\varepsilon_r = 6.0 \pm 0.2$ and $\tan\delta = 0.001$ at 30 GHz. The thicknesses of the substrate layer and the metal layer are 0.095 and 0.015 mm respectively. The antenna is composed of a 16-layer LTCC substrate and occupies a size of L by W. The antenna element consists of four parts: a rectangular radiating patch with a size of l_1 by w_1 (Metal layer 1), a coupling slot with a size of l_2 by w_2 cut onto the broadwall of the SIW (Metal layer 2), a transition layer (Metal layer 3), and a feeding layer at the bottom (Metal layer 4). For feeding the antenna, a co-planar waveguide (CPW) structure is designed on the bottom layer with the inner patch connected to the broadwall of the SIW by a via probe. Compared with other feeding technologies, the proposed CPW to SIW transition has advantages of a wide bandwidth, low loss, and compact size. It is worthwhile to mention that, a six-layer air cavity with a size of l_c by w_c is embedded between Metal layer 1 and Metal layer 2 to enhance the bandwidth and radiation efficiency of the antenna. Ansoft high frequency structure simulator 19.0 has been employed to carry out the simulation and optimisation of the antenna element. The setups of the simulations are as follows: the solution frequency is set as the highest operating frequency and the height of the air box is set as 1/2 wavelength of the lowest operating frequency to achieve more mesh grids. The maximum Delta S is as 0.02. The sweep frequency covers the interesting frequency band from 23 to 28 GHz by interpolating. The general mesh of each unit-cell simulation is around 60,000.

The design steps of the wideband widescan antenna element are summarised as follows. In the first step, the highest operating frequency is generally determined by the inter element spacing and maximum scanning angle to avoid the grating lobe in the interesting space, while it needs some space to accommodate the T/R unit.

$$d \le \lambda_h/(1+\sin\theta_{\max}) \tag{1}$$

where λ_h is the wavelength at the highest operating frequency in free space. $\theta_{\max}$ is the required largest scanning angle.

Furthermore, the lowest operating frequency of the antenna element can be predicted by evaluating the width of the radiating patch (w_1). In the following formula, c is the speed of light in free space, εr is the relative permittivity of LTCC, and f_l is the lowest operating frequency. As the air cavity is embedded in LTCC under the radiating patch, the relative permittivity of the substrate is less than 6.

$$w_1 \approx \frac{c}{4f_l\sqrt{\frac{1+\varepsilon_r}{2}}} \tag{2}$$

At broadside, the impedance matching in the lower frequency band can be improved by enlarging the thickness of metal layer 1. When scanning to large angles, the metal layer 1 should keep low profile to maintain the impedance matching in the upper frequency band. Generally, the thickness of metal layer 1 can be selected from $1/10\lambda$ to $1/4\lambda$. Finally, the dimensions of the via hole and the CPW structure are designed to match the characteristics impedance of the subminiature push-on (SMP) connector.

The unit-cell simulation model has been utilised to study the impedance characteristic of the antenna and the effects of the air cavity. The optimised values of the dimensions are listed in Table 1. The influences on the voltage standing wave ratio (VSWR) response by various dimensions of the air cavity are presented in Figure 2. By tuning the dimensions of the air cavity, the VSWR performance of the antenna element varies significantly. As observed, the VSWR is below 2 at broadside from 23 to 28 GHz when the side length and thickness of the air cavity are 6 mm and 6 layers respectively. The VSWR value increases as the side length of the air cavity reduces from 6 to 1 mm, indicating that the impedance matching can be improved by enlarging the size of the air cavity. Also noticed, the frequency bandwidth is becoming narrower when the thickness of the air cavity decreases from 6-layer to 1-layer. Thus, the bandwidth of the antenna can be increased and the impedance matching over the operating frequency band can be improved by enlarging the volume of the air cavity. For the reliability of the structure, there are two LTCC layers above the embedded air cavity, and the distance between the side wall and the air cavity is 0.5 mm.

The influences on the antenna gain by various dimensions of the air cavity are shown in Figure 3. Simulations have also been implemented to study its effects on radiation patterns. The results are not shown as similar radiation patterns have been observed. The results in Figure 3 have confirmed that, the antenna gain has been significantly enhanced by embedded an air cavity in the LTCC under the radiating patch.

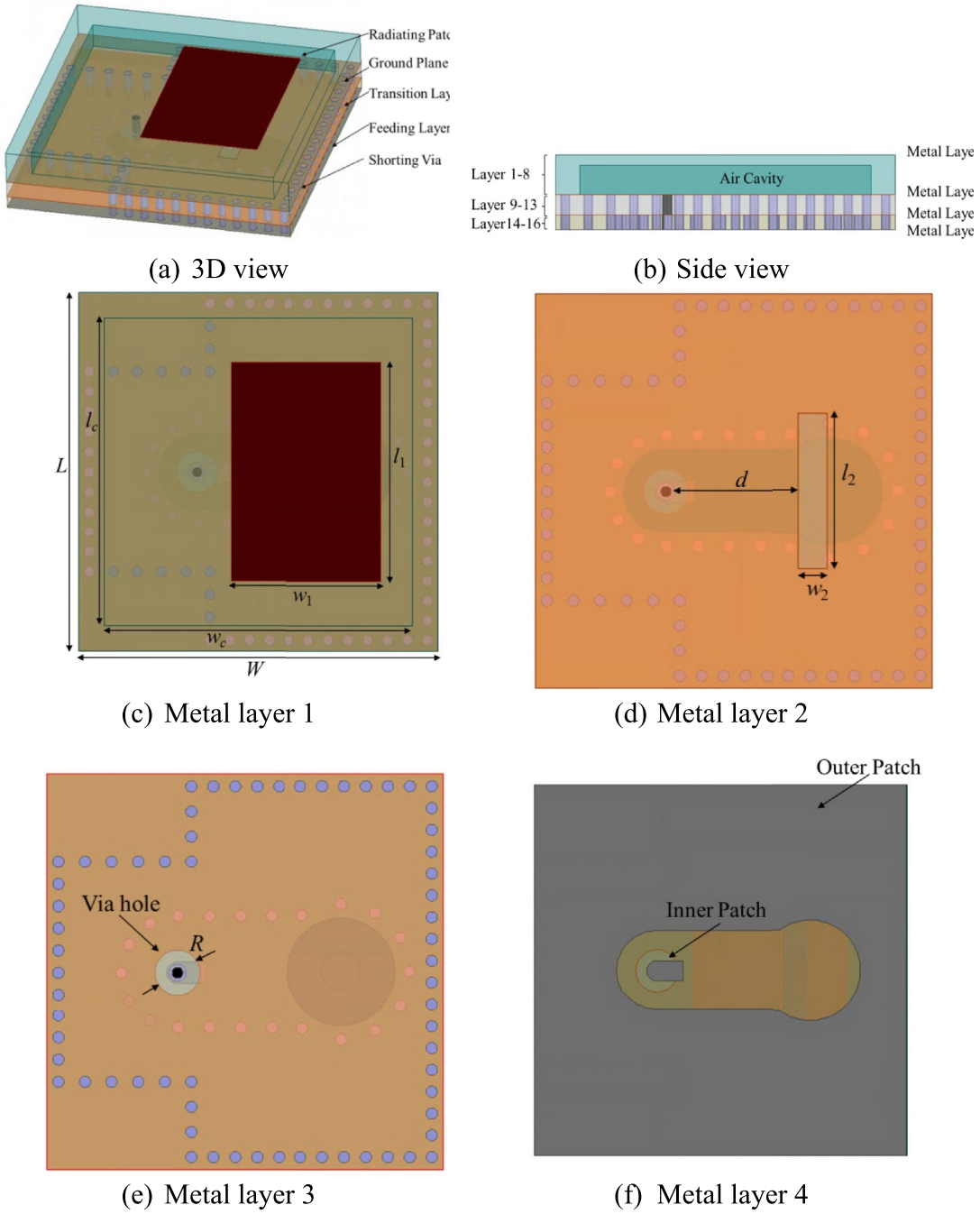

FIGURE 1 The structure and geometry of the proposed antenna element.

TABLE 1 Optimised values of the dimensions (Unit: mm)

L	W	l_1	w_1	l_c	w_c
7	7	4.3	2.9	6	6
l_2	w_2	d	R		
2.7	0.5	2.3	0.8		

The simulated active VSWRs versus frequency at different scanning angles are shown in Figure 4. As noticed, the active VSWR at broadside across the frequency range from 23 to 28 GHz is less than 2. As the scanning angle is up to 45°, the active VSWRs are less than 2.5 and 2.2 in the H- and E-plane respectively. The obtained results can indicate that the proposed antenna array features the wideband and widescan characteristics.

3 | ANTENNA ARRAY DESIGN

After indication of good performance in an infinite array environment, a 49-port prototype array with a size of 49 mm by 49 mm was fabricated and measured. The inter element spacing of the array are 7 mm by 7 mm in the two directions.

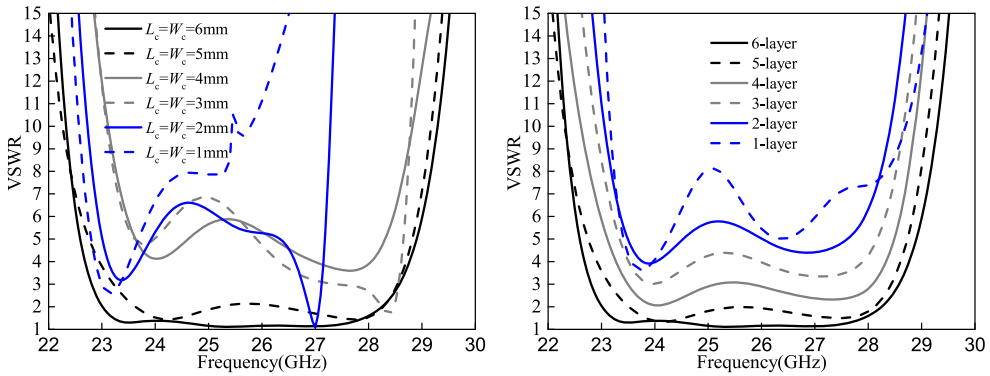

FIGURE 2 The effects on the impedance matching at broadside by the sizes and thicknesses of the air cavity.

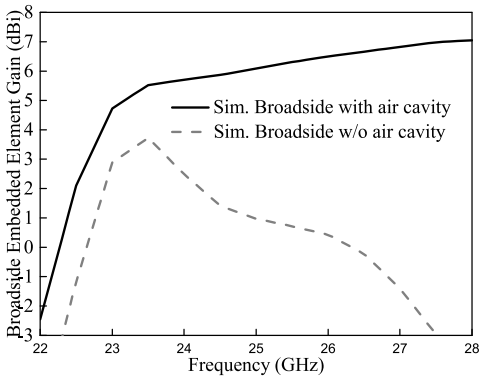

FIGURE 3 The effects on the antenna gain by the air cavity.

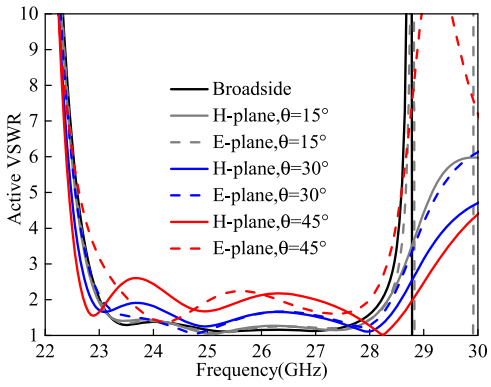

FIGURE 4 Simulated active VSWRs versus frequency in the E- and H-plane at various scanning angles. VSWR, voltage standing wave ratio

The structure and photo of the proposed antenna array are presented in Figures 5 and 6 respectively. In the backview of the structure, a surface-mounted SMP connector was soldered to each feeding port of the array. The diagram of the fabrication of the antenna array is shown in Figure 7. The LTCC structure was first laminated at high pressure in two separate parts, namely layers 1-8 and layers 9–16. A thin layer of adhesive was utilised to glue the pre-laminated parts together. During the cofiring process, the adhesive burns off efficiently and the dielectric layers are sintered together. It is worthwhile to mention that, small holes have been drilled in the top layer in the last step to avoid any deformation of the cavity due to the pressure difference. The embedded air cavity can enhance the bandwidth and radiation efficiency of the antenna array. Due to the proposed fabrication technology, the reliability can be maintained though a large-size LTCC substrate with air cavities has been fabricated.

Active impedance measurements of a central element were carried out using a network analyser. S-parameter mutual coupling measurements to all other elements were collected, while all other ports are matched. The active reflection coefficient of the central element has been calculated using the formula in ref [10].

$$\Gamma_{pq}(\theta,\varphi)=\sum_{m=1}^{M}\sum_{n=1}^{N}S_{mn,pq}e^{-jk\left([m-p]D_x u+[n-q]D_y v\right)} \quad (3)$$

where (θ,φ) is the array scan direction, $u = k\sin\theta\cos\varphi$ and $v = k\sin\theta\sin\varphi$ are the u-v coordinates, $k = 2\pi/\lambda$ is the free-space wavenumber, $S_{mm,pq}$ are the measured S-parameter mutual coupling between elements mn and pq, and $M = 7$, $N = 7$, and $D_x = L$, $D_y = W$ are the number of elements in the two directions and their lattice spacing respectively. Hence, the active VSWR can be expressed as

$$\mathrm{VSWR}_{pq}(\theta,\varphi)=\frac{1+\Gamma_{pq}(\theta,\varphi)}{1-\Gamma_{pq}(\theta,\varphi)} \quad (4)$$

The measured active VSWRs at various scanning angles in the H- and E-planes for the central element are shown in Figure 8 alongside infinite array simulations. As observed, the measured active VSWRs from 23 to 28 GHz in the H- and E-planes are below 2.5 and 2 respectively, when scanning up to 45°. The embedded element pattern is an alternative indication of the scan performance for a finite array. The measurement of the radiation patterns for the central element has been conducted by using planar near-field antenna measurement system when other ports terminated in 50 Ω. The planar near-field antenna test has been conducted by using an industrial 6-axis

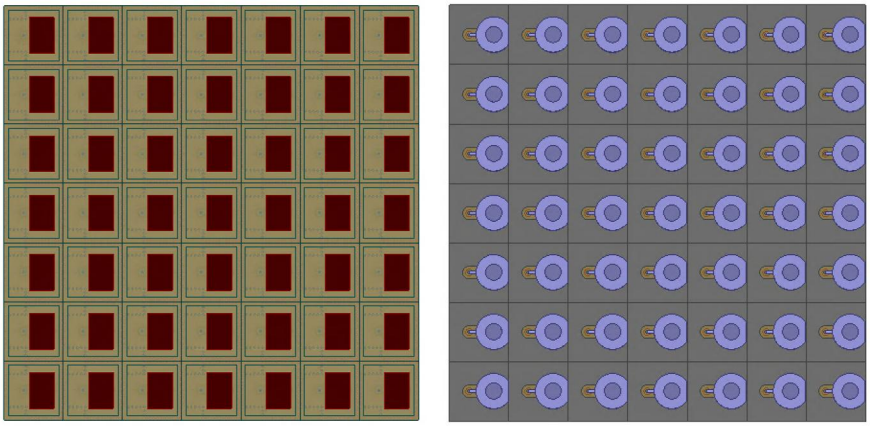

FIGURE 5 Structure of the proposed 7 by 7 antenna array.

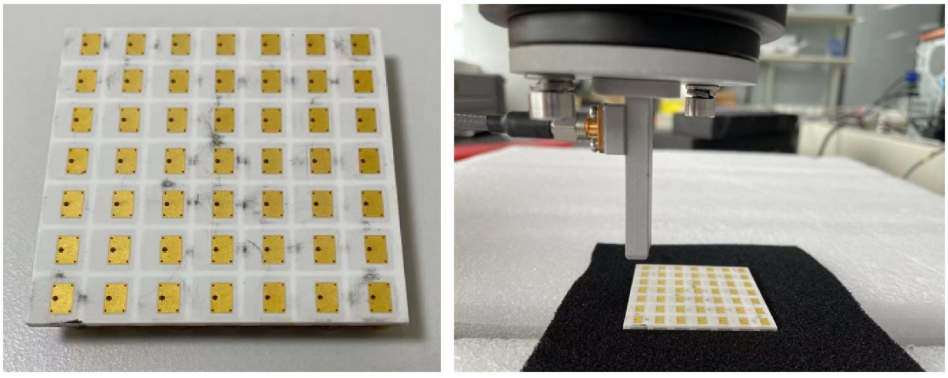

FIGURE 6 The photo of the fabricated prototype.

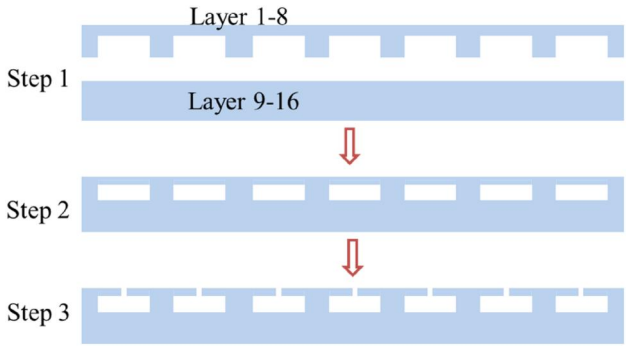

FIGURE 7 The steps of the fabrication of the antenna array.

robot, as shown in Figure 6(right). Compared with far-field measurement, near-field measurement has the advantages of avoiding signal transmitting attenuation and high test efficiency. The near-field measurement system is composed of six rotary axes embedded in the robot which are coupled with an external axis on which the waveguide probe is mounted. The six rotational axes are combined in motion to result in an arbitrary position within the mechanical reach of the robot. The design is similar as the system based on NSI-MI technologies [22]. In the measurement, a waveguide probe is scanning a rectangular plane in the near-field of the antenna array and obtaining the amplitude and phase at each scanning point on the plane. Accordingly, the far field patterns and gain of the antenna array can be determined by transforming the amplitudes and phases of the near fields. In our test, the distance between the probe and the array is 40 mm, and the scanning plane is 150 mm by 150 mm. These measurements aim to highlight the proposed array's ability of wide-angle scanning in both E- and H-planes. The measured embedded element patterns of the central element at different frequencies in both E- and H-planes are presented in Figure 9. The results can confirm that measurements and simulations within the required scanning angles are in reasonable agreement with some differences beyond the required scanning angles; these are mainly due to the near-field test method. It is also worthwhile to mention that the pattern ripples are due to the finite size of the array and will decreases in a larger array.

Moreover, the measured radiation patterns of the array with various scanning angles at different frequencies are illustrated in Figure 10. The results can further confirm that the proposed antenna array can scan up to 45° in both E- and H-planes. It is also noticed that, the grating lobes will be observed when scanning up to 45° while the levels are lower than the main lobe. The measured and simulated broadside embedded element gains versus frequency are shown in Figure 11 with the theoretical ideal gain used as a reference. The average gain drop between the measured result and the theoretical gain is 0.73dB; a maximum drop of 1.15dB in the

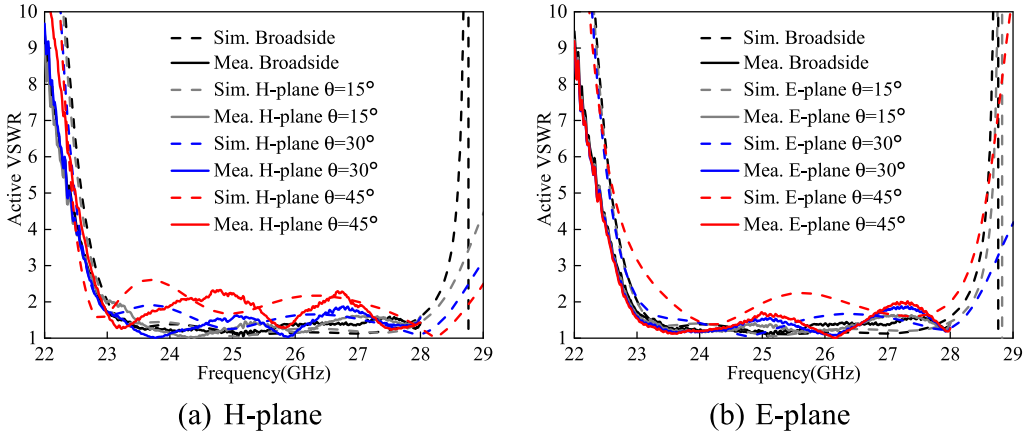

FIGURE 8 Simulated and measured active VSWRs in the H- and E-planes. VSWR, voltage standing wave ratio

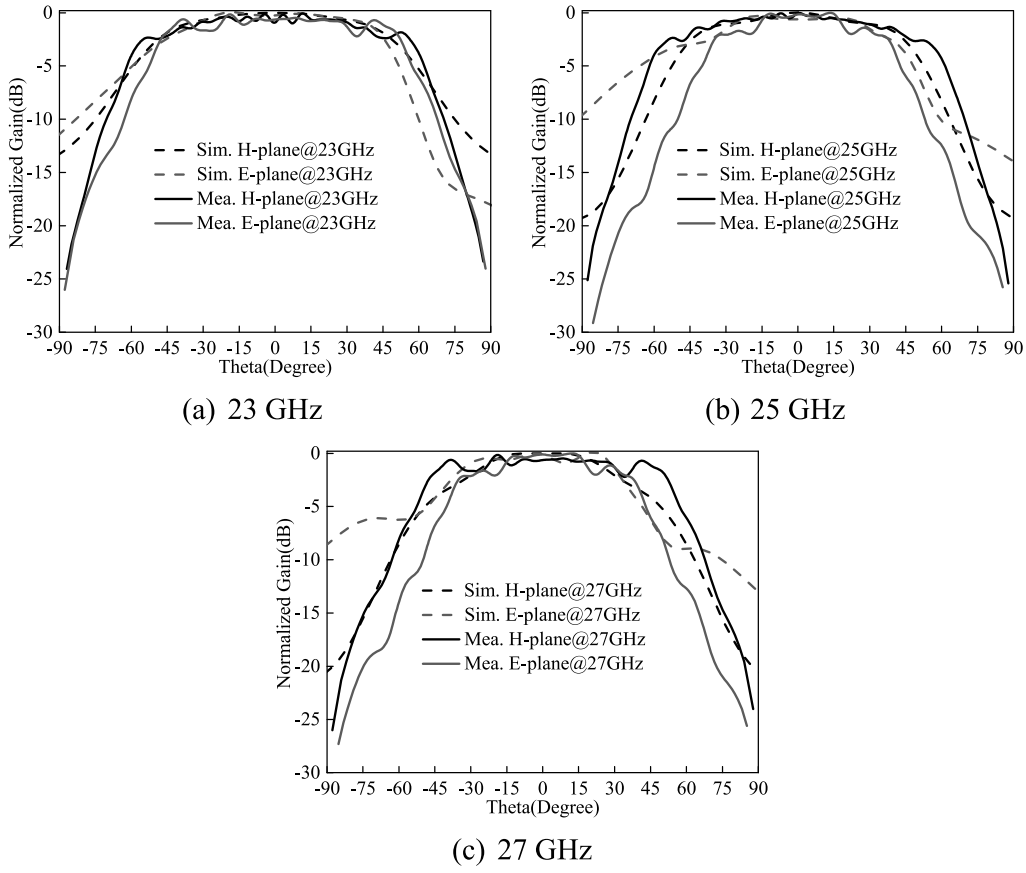

FIGURE 9 Simulated and measured embedded element patterns at various frequencies.

measured gain is observed in the lower frequency band. Thus, the proposed array antenna has achieved a high radiation efficiency of around 84%.

For further demonstration, the performance comparisons with other recently reported mm-wave antenna arrays are listed in Table 2. As observed, most researchers have focussed on the designs of mm-wave antenna arrays with broadside radiation [11–16, 18–20]. These mm-wave antenna arrays have been fabricated by using PCB technology [11–14, 17], milling technology [16], and LTCC technology [15, 18–21]. The arrays using PCB technology are normally composed of several layers (2–3) of poly tetra fluoroethylene (PTFE) substrates with one layer for feeding and other layers for radiating. The advantages of the PCB-based arrays include low price, low dielectric loss and easy fabrication, while only several layers can be fabricated in practice. In addition, the PTFE substrate has a high thermal expansion coefficient indicating that T/R modules cannot be soldered directly with the arrays due to the mismatch of the

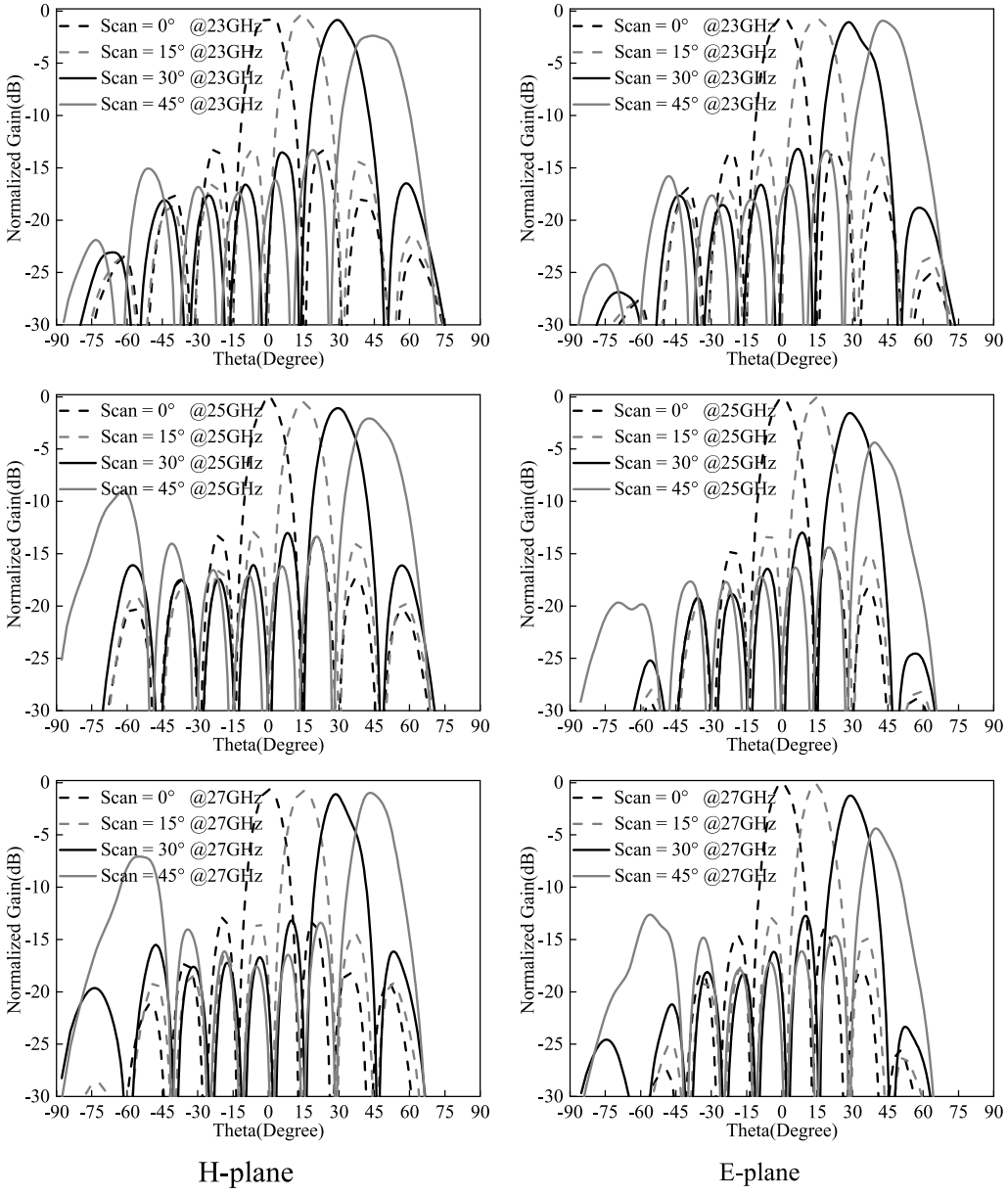

FIGURE 10 Measured radiation patterns of the array at various frequencies.

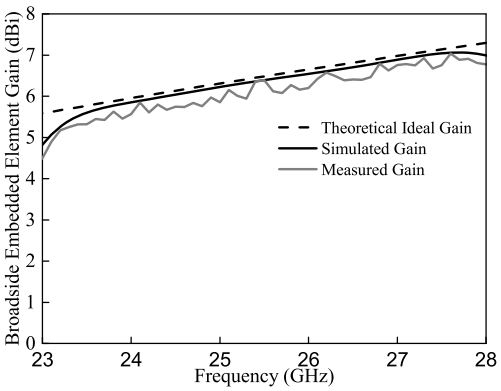

FIGURE 11 Comparison among measured broadside embedded element gain, the theoretical gain and simulated antenna gain.

two materials. The gap waveguide-fed mm-wave array [16] has achieved a high gain and radiation efficiency by milling technology. The advantages of milling technology are low loss, high efficiency, and high reliability while the cost is very high and the volume is bulky. Compared with these two technologies, LTCC technology is an excellent candidate for designing millimetre-wave antennas due to its merits of multilayer configuration, flexible metallisation, and low fabrication tolerance. The antennas and arrays designed by LTCC technology have been reviewed and summarised in [21]. However, the high permittivity and Q-factor of the LTCC substrate at millimetre-wave frequency leads to significant losses and narrow bandwidth. Generally, the relative bandwidth of the LTCC antenna is less than 5% and the radiation efficiency is less than 70% [18, 20]. Due to the differential feeding technique, the bandwidth of the

TABLE 2 Performance comparisons with other reported mm-wave arrays

Ref.	Array scale	Centre freq. (GHz)	Imp. BW (%)	Scan	Feeding
[11]	4 × 4	27.75	17.7	N	Microstrip to SIW
[12]	4 × 4	28	8.5	N	TE_{20}-mode SIW
[13]	1 × 8	28.45	8.08	N	SIW
[14]	6 × 7	27.7	6.3	N	Stripline to microstrip
[15]	4 × 4	27	18.5	N	Probe
[16]	16 × 16	28	5.2	N	Gap waveguide
[17]	16 × 16	26	15.38	Y	SIW
[18]	16 × 16	29	4	N	Laminated waveguide
[19]	4 × 4	37	13.96	N	Laminated waveguide
[20]	Nan	60	3.4	N	Waveguide
This work	7 × 7	25.5	19.6	Y	CPW to SIW

Abbreviations: BW, bandwidth; CPW, co-planar waveguide; SIW, substrate integrated waveguide.

LTCC array reaches around 18.5%. The bandwidth of a 4 × 4 LTCC array has been enhanced to 13.96% by an artificial magnetic conductor due to its in-phase characteristics. Compared with other mm-wave arrays, the proposed array has achieved a relative bandwidth of 19.6% by embedding an air cavity in the LTCC substrate.

On the other hand, the efficiency of an array antenna is a significant consideration for the mm-wave band. Compared with microstrip lines, stripline [14], and SIW [11–13, 17] feeding networks are more appropriate for the mm-wave band due to less loss. Moreover, the SIW feeding technology is more popular due to its single layer while the stripline needs two layers of substrates. The transition to SIW also needs to be taken into consideration, especially for mm-wave applications. The coaxial waveguide transition [12, 18, 19] has been widely employed in SIW-fed antenna test, while it is not suitable for mm-wave phased array antenna due to its bulky size. The proposed CPW to SIW transition in our work has advantages of a wide bandwidth, low loss, and compact size.

Finally, most published mm-wave arrays have been designed for broadside radiation. In ref. [17], the proposed 16 by 16 antenna array can switch to different angles while its impedance bandwidth is less than 16%. Compared with recently published work, the proposed antenna array has achieved the wideband widescan performance with a larger bandwidth.

4 | CONCLUSION

The design of a 7 × 7 SIW-fed antenna array on LTCC with capabilities of wide-angle scanning in the frequency band from 23 to 28 GHz has been presented. The antenna element consists of four parts: a rectangular radiating patch, a coupling slot cut onto the broadwall of the SIW, a transition layer, and a feeding layer at the bottom. A six-layer air cavity has been embedded to increase the bandwidth and radiation efficiency of the antenna. The effects of the air cavity have been extensively studied. Furthermore, a prototype of a 7 × 7 array has been fabricated and characterised in terms of active VSWR and embedded element patterns in both E- and H-planes. The measured results have shown that active VSWRs of the proposed antenna array from 23 to 28 GHz in the H- and E-planes are below 2.5 and 2 for scanning up to 45°. The measured embedded element patterns match well with the simulated results within the required scanning angles and no significant gain drop is observed. Compared with the theoretical ideal gain, the average gain drop is around 0.73dB for the measured embedded element gain, indicating a high radiation efficiency of 84%.

AUTHOR CONTRIBUTION

Fuguo Zhu: Conceptualisation; Methodology; Resources; Validation; Writing – original draft. **Yuefei Wang**: Formal analysis; Resources. **Jinping Zhang**: Methodology. **Lei Sun**: Project administration. **Zhipeng Zhou**: Project administration. **Steven Gao**: Supervision.

CONFLICTS OF INTEREST

The authors declare no conflict of interest.

DATA AVAILABILITY STATEMENT

Data available in article supplementary material.

ORCID

Fuguo Zhu https://orcid.org/0000-0003-1882-7674

REFERENCES

1. Park, S.J., Park, S.O.: LHCP and RHCP substrate integrated waveguide antenna arrays for millimeter-wave applications. IEEE Antenn. Wireless Propag. Lett. 16, 601–604 (2017). https://doi.org/10.1109/lawp.2016.2594081
2. Li, Y., et al.: Axial ratio bandwidth enhancement of 60-GHz substrate integrated waveguide-fed circularly polarized LTCC antenna array. IEEE Trans. Antenn. Propag. 60(10), 4619–4626 (2012). https://doi.org/10.1109/tap.2012.2207343

3. Qian, J., et al.: Heatsink antenna array for millimeter-wave applications. IEEE Trans. Antenn. Propag. 68(11), 7664–7669 (2020). https://doi.org/10.1109/tap.2020.2979194
4. Li, P., et al.: 60 GHz dual-polarized high-gain planar aperture antenna array based on LTCC. IEEE Trans. Antenn. Propag. 68(4), 2883–2894 (2020). https://doi.org/10.1109/tap.2019.2957095
5. Qian, J., et al.: Integration of S/Ka/D-band antennas in LTCC with a cylindrical radome for triband applications. IEEE Trans. Antenn. Propag. 67(9), 5781–5789 (2019). https://doi.org/10.1109/tap.2019.2916559
6. Lamminen, A.E.I., Vimpari, A.R., Saily, J.: UC-EBG on LTCC for 60-GHz frequency band antenna applications. IEEE Trans. Antenn. Propag. 57(10), 2904–2912 (2009). https://doi.org/10.1109/tap.2009.2025401
7. Yeap, S.B., Chen, Z.N., Qing, X.: Gain-enhanced 60-GHz LTCC antenna array with open air cavities. IEEE Trans. Antenn. Propag. 59(9), 3470–3473 (2011). https://doi.org/10.1109/tap.2011.2161549
8. Panther, A., et al.: A wideband array of stacked patch antenna using embedded air cavities in LTCC. IEEE Microw. Wireless Compon. Lett. 15(12), 916–918 (2005). https://doi.org/10.1109/lmwc.2005.859944
9. Lamminen, A.E.I., Saily, J., Vimpari, A.R.: 60-GHz patch antennas and arrays on LTCC with embedded-cavity substrate. IEEE Trans. Antenn. Propag. 56(9), 2865–2874 (2008). https://doi.org/10.1109/tap.2008.927560
10. Logan, J.T., et al.: A new class of planar ultrawideband modular antenna arrays with improved bandwidth. IEEE Trans. Antenn. Propag. 66(2), 692–701 (2018). https://doi.org/10.1109/tap.2017.2780878
11. Xu, J., et al.: Wideband, low-profile patch array antenna with corporate stacked microstrip and substrate integrated waveguide feeding structure. IEEE Trans. Antenn. Propag. 67(2), 1368–1373 (2019). https://doi.org/10.1109/tap.2018.2883561
12. Jin, H., et al.: Millimeter-wave TE20-mode SIW dual-slot-fed patch antenna array with a compact differential feeding network. IEEE Trans. Antenn. Propag. 66(1), 456–461 (2018). https://doi.org/10.1109/tap.2017.2767644
13. Park, S.-J., Shin, D.-H., Park, S.-O.: Low side-lobe substrate integrated-waveguide antenna array using broadband unequal feeding network for millimeter-wave handset device. IEEE Trans. Antenn. Propag. 64(3), 923–932 (2016). https://doi.org/10.1109/tap.2015.2513075
14. Dzagbletey, P.A., Jung, Y.-B.: Stacked microstrip linear array for millimeter-wave 5G baseband communication. IEEE Antenn. Wireless Propag. Lett. 17(5), 780–783 (2018). https://doi.org/10.1109/lawp.2018.2816258
15. Zhang, Y., et al.: Broadband dual-polarized differential-fed filtering antenna array for 5G millimeter-wave applications. IEEE Trans. Antenn. Propag. 70(3), 1989–1998 (2022). https://doi.org/10.1109/tap.2021.3118800
16. Ran, J., et al.: High-gain and low-loss dual-polarized antenna array with reduced sidelobe level based on gap waveguide at 28 GHz. IEEE Antenn. Wireless Propag. Lett. 21(5), 1022–1025 (2022). https://doi.org/10.1109/lawp.2022.3155566
17. Kong, W., et al.: 2-D orthogonal multibeam antenna array for 5G millimeter-wave applications. IEEE Trans. Microw. Technol. Tech. 70(5), 2815–2824 (2022). https://doi.org/10.1109/tmtt.2022.3162113
18. Huang, Y., et al.: An integrated LTCC millimeter-wave planar array antenna with low-loss feeding network. IEEE Trans. Antenn. Propag. 53(3), 1232–1234 (2005). https://doi.org/10.1109/tap.2004.842588
19. Yang, W.C., et al.: High-gain and low-loss millimeter-wave LTCC antenna array using artificial magnetic conductor structure. IEEE Trans. Antenn. Propag. 63(1), 390–395 (2015). https://doi.org/10.1109/tap.2014.2364591
20. She, Y., et al.: LTCC oversized rectangular waveguide slot array antenna with air-layer in the radiating part in the millimeter-wave band. IEEE Trans. Antenn. Propag. 61(4), 1777–1783 (2013). https://doi.org/10.1109/tap.2012.2237008
21. Ullah, U., et al.: Antenna in LTCC technologies: a review and the current state of the art. IEEE Antenn. Propag. Mag. 57(2), 241–260 (2015). https://doi.org/10.1109/map.2015.2414668
22. Hatzis, J., Pelland, P., Hindman, G.: Implementation of a combination planar and spherical near-field antenna measurement system using an industrial 6-aix robot. In: Proceedings 38th Annual Symposium Antenna Measurement Techniques Association (AMTA), pp. 1–6, Austin (2016)

How to cite this article: Zhu, F., et al.: Design of a Low temperature cofired ceramic wideband WideScan antenna array for millimetre-wave applications. IET Microw. Antennas Propag. 1–9 (2022). https://doi.org/10.1049/mia2.12316